Transition to quantum turbulence in a Bose-Einstein condensate through the bending-wave instability of a single-vortex ring

T.-L. Horng,[1] C.-H. Hsueh,[2] and S.-C. Gou[2]
[1]*Department of Applied Mathematics, Feng Chia University, Taichung 40724, Taiwan*
[2]*Department of Physics, National Changhua University of Education, Changhua 50058, Taiwan*
(Received 25 April 2008; published 30 June 2008)

We investigate the dynamics of an unstable vortex ring in a pancake-shaped Bose-Einsten condensate by solving the Gross-Pitaevskii equation numerically. It is found that a quasisteady turbulent state with long relaxation time can be achieved through the disruption of a perturbed vortex ring in the condensate owing to the bending-wave instability. We verify that this quantum turbulent state is characterized by Kolmogorov energy spcetrum.

DOI: 10.1103/PhysRevA.77.063625 PACS number(s): 03.75.Kk, 47.32.C−, 47.37.+q, 67.25.dk

I. INTRODUCTION

Ever since the discovery of turbulent motion in the superfluid ^{4}He with the thermal counterflow apparatus, the quantum turbulence (QT) has become an important and active subject in low-temperature physics [1]. In the past few decades, QT based on thermal counterflow has been thoroughly studied, and many fundamental properties of this type of turbulence are now well understood. However, due to the lack of classical analogs, the counterflow turbulence was believed to have no direct connections with the classical turbulence (CT). More specifically, the difference between QT and CT should be exposed from the fundamental aspect of the vortex structure: the vorticity is quantized in a superfluid, but is continuously distributed in a classical fluid. On this basis, QT is ascribed to the tangle of quantized vortex filaments whose dynamics differ from that of the chaotic but continuous vorticity of CT [2,3].

More recently, QT in superfluid ^{4}He without using thermal counterflow has been achieved experimentally [4,5]. Surprisingly, it has been found that QT produced in such cases does possess properties very similar to those of CT, despite the fundamental difference between these two types of turbulence. In particular, the Kolmogorov's $-5/3$ power law [6], which is derived based on the assumption that the fully developed turbulence is statistically self-similar at different scales, has been also observed in QT [4,5] and verified numerically [7–9]. These findings have aroused considerable interest in exploring the possible connection between QT and CT. Since QT has been well studied, it is expected that via the study of QT one may pave a way towards a better understanding for the less understood CT.

On the other hand, the low-temperature physics has entered a new era in the past decade, owing to the astounding experimental advances in exploring the ultracold atomic physics in the laser cooled and trapped alkali gases. By virtue of the close relationship between superfluid behavior and quantized vorticity in liquid helium and atomic Bose-Einstein condensate (BEC) [10], the QT in the trapped BEC has been addressed in the last few years. In these pioneering theoretical studies, the QT is predicted to occur in the following cases: in the evolving stage prior to the nucleation of vortex lattice in a rotating condensate [11,12], in the collision of two condensates [13], and in the combined rotations around two axes of a condensate [14].

In this paper, we report another pathway to QT in a trapped BEC via the disruption of an unstable vortex ring. This work is motivated by our previous studies on the motion of a vortex ring in a trapped BEC [15]. Using the modified vortex-filament formalism derived from the time-dependent Gross-Pitaevskii (GP) equation [16], together with the idea that the trapping potential causes vortex stretching, we have concluded that the azimuthally wavy distortions (the bending waves) on the filament of the vortex ring can be amplified exponentially under certain circumstances, whence leads to the disruption of the vortex ring. Specifically, for the cylindrical trapping potential, $V(\mathbf{r})=m\omega_\perp^2(r^2+\lambda^2z^2)/2$, we have shown analytically that a slightly oblate geometry, $1 \leqslant \lambda \leqslant 2$, is required to prevent the vortex ring from becoming unstable due to the bending-wave instability.

It should be noted that although we have used the vortex-filament model to determine the stability condition for the motion of a vortex ring in the trapped BEC, this approach does not provide complete information about the dynamics of the condensate after the vortex ring is disrupted. One important reason is that, to acquire the integrability of the motion equations for the vortex filaments, we have assumed the vortex lines to be infinitely slender filaments. This assumption, however, excludes the interaction between vortices, such as the vortex reconnection, as well as that between vortices and sound field (density fluctuations). In fact, the vortex reconnection, which plays a central role in converting the vortical energy into the sound energy, is of fundamental importance that is indispensable in creating QT in superfluids. In any case, being short of these dynamical ingredients, the vortex-filament model can only serve to reveal some qualitative features of the motion of vortex ring. To probe into the full dynamics of the system, we must resort to the numerical integration of the GP equation

$$i\frac{\partial}{\partial t}\Psi(\mathbf{r},t)=\left(-\frac{\nabla^2}{2}+V(\mathbf{r})+g|\Psi(\mathbf{r},t)|^2\right)\Psi(\mathbf{r},t) \qquad (1)$$

with a perturbed vortex ring placed initially inside the condensate. Here the condensate wave function $\Psi(\mathbf{r},t)$ is normalized by $\int|\Psi(\mathbf{r},t)|^2d\mathbf{r}=1$, and $g=4\pi aN$ is the coupling

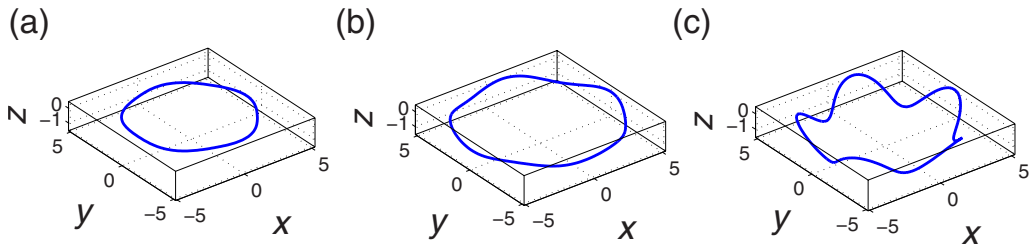

FIG. 1. (Color online) Demonstration for the disrupiton of a vortex ring in a pancake-shaped BEC according to the results of Ref. [15]. (a) The initially perturbed vortex ring. (b) Growth of the disturbance. (c) Formation of hairpins.

strength, where N is the total number of atoms in the condensate and a is the s-wave scattering length. Note that the GP equation is given in the dimensionless form, in which the length, time, and energy are, respectively, scaled in units of $(\hbar/m\omega_\perp)^{1/2}$, $\omega_\perp^{-1}$, and $\hbar\omega_\perp$. The details of the numerical calculations will be presented in the following sections.

II. DESCRIPTION OF THE MODEL

Before proceeding to the numerical simulation, we remark briefly on the construction of an initial vortex ring configuration in an inhomogeneous BEC. For simplicity, we shall consider an axisymmetrically oriented planar vortex loop, which is disposed on the xy plane at $t=0$ with its radius sinusoidally disturbed. Let the radius of the unperturbed ring be R_0 and the amplitude of the bending wave be η. In the cylindrical coordinates (r,ϕ,z), the core axis of the bent ring is described by $r=R(\phi)$, $z=0$, where $R(\phi)=R_0+\eta\cos(n\phi)$, with n being an integer. Next we define a local core-centered polar coordinate (ζ,τ) on the semi-infinite plane, $0\leqslant r<\infty$ and $-\infty<z<\infty$, along the directional angle ϕ, where

$$\zeta(\mathbf{r})=\sqrt{[r-R(\phi)]^2+z^2},\quad \tau(\mathbf{r})=\tan^{-1}\frac{z}{r-R(\phi)}. \tag{2}$$

Following the method in Ref. [17], we introduce the trial form, $\Psi(\mathbf{r},t)=\exp(-i\varepsilon t)\exp[i\kappa\tau(\mathbf{r})]\psi(\mathbf{r})$, of the condensate wave function, where κ is an integer indicating the quantum of circulation and ε is a real number. Substituting $\Psi(\mathbf{r},t)$ into Eq. (1), we obtain the time-independent GP equation of $\psi(\mathbf{r})$,

$$\left(-\frac{[\nabla-i\mathbf{A}(\mathbf{r})]^2}{2}+V(\mathbf{r})+g|\psi(\mathbf{r})|^2\right)\psi(\mathbf{r})=\varepsilon\psi(\mathbf{r}), \tag{3}$$

where $\mathbf{A}(\mathbf{r})=-\kappa\nabla\tau(\mathbf{r})$, which is explicitly expressed as

$$\mathbf{A}(\mathbf{r})=-\kappa\left[\frac{z}{\zeta^2}\hat{\mathbf{r}}+\frac{n\eta z\sin(n\phi)}{r\zeta^2}\hat{\phi}-\frac{r-R(\phi)}{\zeta^2}\hat{\mathbf{z}}\right]. \tag{4}$$

Finally, the desired initial vortex configuration is restored by $\Psi(\mathbf{r},0)=\exp[i\kappa\tau(\mathbf{r})]\psi_0(\mathbf{r})$, where $\psi_0(\mathbf{r})$ is the lowest energy state of Eq. (3) which can be numerically obtained by imaginary time propagation of Eq. (3).

To numerically integrate Eq. (1), we use the method of lines with spatial discretization by Fourier pseudospectral method and time integration by adaptive Runge-Kutta method of order 2 and 3 (RK23). Inspired by our previous results [15], we assume that a bent, singly quantized ($\kappa=-1$) vortex ring filament parametrized by $R_0=4$, $\eta=0.1$, $n=5$ is initialized in a pancake-shaped BEC characterized by $\lambda=5$, $R_\perp=8$. Here $R_\perp=\sqrt{2\mu}$ is the transverse Thomas-Fermi radius of the trapped BEC, and μ denotes the chemical potential for the vortex-free condensate. Accordingly, such a ring configuration is predicted to be unstable by vortex-filament method as shown by the hairpins formation in Fig. 1(c). When the disturbance is further amplified into highly nonlinear regime, the runaway stretching of the vortex filament occurs. Consequently, the disruption of the vortex ring is indicated by the divergence of the total length of the filament and further exploration of dynamics is stopped by the limitation of the vortex-filament method.

III. RESULTS AND DISCUSSIONS

Now, using the aforementioned method for initializing the vortex ring wave function together with the same parameters given in Fig. 1, the time evolution of the vortex ring is shown in Figs. 2(a)–2(l) by the isosurfaces of $|\Psi(\mathbf{r},t)|^2$ at different time. We see that, in Figs. 2(b)–2(d) the vortex ring does evolve into the hairpin structure which is qualitatively similar to that of Fig. 1(c). Note that although the vortex ring appears disconnected in Figs. 2(c) and 2(d), it remains connected in an isosurface of much smaller densities. Nevertheless, as the vortex ring continues to deform, it actually breaks into multiple vortex filaments at a later moment. Afterwards, these fractured vortex filaments are driven to tangle, reconnect, and deform successively, etc., initiating the scenario of transition to turbulence. Moreover, as time progresses, the vortex filaments disappear gradually, and in the meantime, the density isosurface becomes more and more wrinkled. Af-

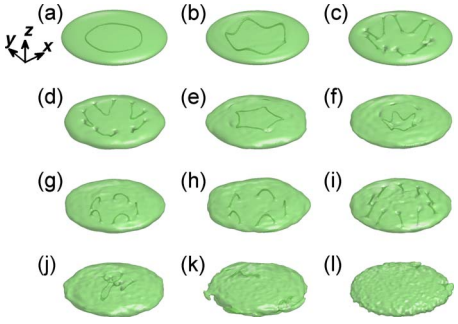

FIG. 2. (Color online) Perspective view of the isosurface for $|\Psi|^2=9\times10^{-4}$ at (a) $t=0$, (b) $t=3$, (c) $t=4$, (d) $t=5$, (e) $t=6.25$, (f) $t=8.25$, (g) $t=9.75$, (h) $t=10.5$, (i) $t=12$, (j) $t=16.75$, (k) $t=20$, and (l) $t=50$. The initial central density is $|\Psi(\mathbf{r}=0)|^2=5.9\times10^{-3}$.

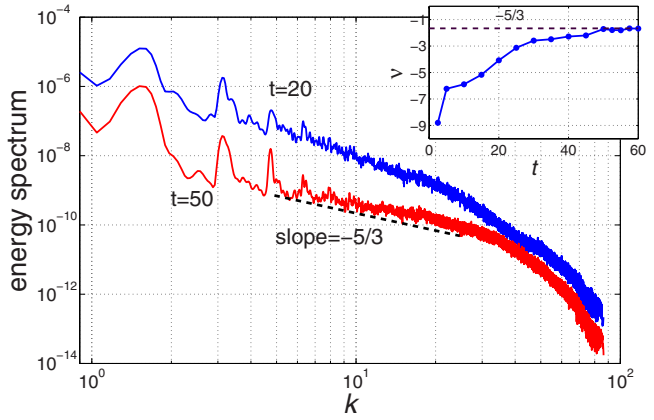

FIG. 3. (Color online) Incompressible kinetic energy spectra $\mathcal{E}_k^i(k)$ at $t=20$ and 50. For comparison, $\mathcal{E}_k^i(k)$ at $t=20$ is deliberately multiplied by 10 to visually separate from that for $t=50$. The consistency between $\mathcal{E}_k^i(k)$ and Kolmogorov spectrum is indicated. Inset: time evolution of the exponent ν.

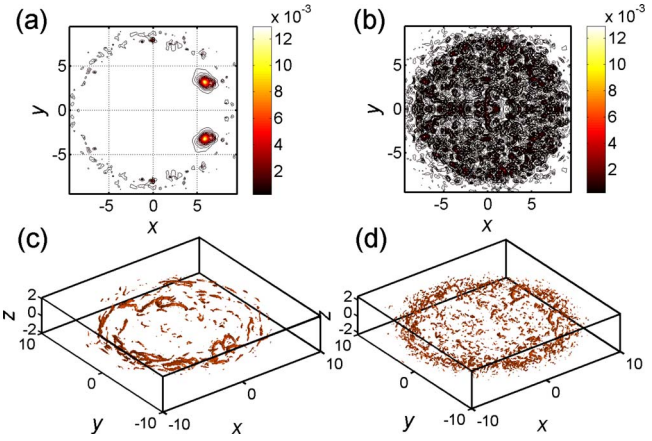

FIG. 4. (Color online) Contour plot for the kinetic energy densities (a) incompressible field and (b) compressible field, on the xy plane at $t=50$, and the perspective view of three-dimensional spatial distribution of vortices at (c) $t=20$ and (d) $t=50$.

ter a sufficiently long period, the condensate is expected to enter the turbulent regime as shown by Fig. 2(l).

To identify whether the state in Fig. 2(l) is turbulent, we check if its incompressible kinetic energy spectrum obeys Kolmogorov's $-5/3$ law. To this end, it is more convenient to write the condensate wave function in the form $\Psi(\mathbf{r},t)=\sqrt{\rho(\mathbf{r},t)}\exp[i\varphi(\mathbf{r},t)]$. As a result, the total energy is expressed as the sum of four terms, namely, $E_{tot}=E_k+E_q+E_{trap}+E_{int}$, where $E_k=\frac{1}{2}\int|\sqrt{\rho}\nabla\varphi|^2d\mathbf{r}$ denotes the superfluid kinetic energy, $E_q=\frac{1}{2}\int|\nabla\sqrt{\rho}|^2d\mathbf{r}$ the quantum pressure energy, $E_{trap}=\int\rho Vd\mathbf{r}$ the trap energy, and $E_{int}=\frac{1}{2}\int g\rho^2d\mathbf{r}$ is the interaction energy. Following Ref. [8], we split the vector field $\sqrt{\rho}\nabla\varphi$ into the solenoidal and irrotational parts, or correspondingly, the incompressible and compressible parts, i.e., $\sqrt{\rho}\nabla\varphi=(\sqrt{\rho}\nabla\varphi)^i+(\sqrt{\rho}\nabla\varphi)^c$, where $\nabla\cdot(\sqrt{\rho}\nabla\varphi)^i=0$ and $\nabla\times(\sqrt{\rho}\nabla\varphi)^c=0$. Thus, the compressible and incompressible kinetic energies are defined by $E_k^{i,c}=\frac{1}{2}\int d\mathbf{r}|(\sqrt{\rho}\nabla\varphi)^{i,c}|^2$. Physically, E_k^i and E_k^c correspond to the kinetic energies in the vortices and sound waves, respectively. Since the compressible and incompressible fields are mutually orthogonal, it follows that $E_k=E_k^i+E_k^c$. The kinetic energy spectrum as a function of wave number k is defined by [8]

$$\mathcal{E}_k^{i,c}(k)=\frac{1}{2}\int k^2\sin\theta d\theta d\phi\left|\int e^{i\mathbf{k}\cdot\mathbf{r}}(\sqrt{\rho}\nabla\varphi)^{i,c}\frac{d\mathbf{r}}{(2\pi)^3}\right|^2 \tag{5}$$

such that $E_k^{i,c}=\int_0^\infty\mathcal{E}_k^{i,c}(k)dk$. In Eq. (5), the integral over the k shell in the momentum space is accomplished by numerically summing over the grid points with $|\mathbf{k}|=k$. From the outcome of numerical computations, we find that the incompressible spectrum always obeys a power law, $\mathcal{E}_k^i(k)\propto k^\nu$, over a certain range of k in the development of turbulence. In Fig. 3, the time-varying exponent ν approaches to the limiting value $-5/3$ asymptotically. Also shown in the same figure, the details of $\mathcal{E}_k^i(k)$ at $t=20$ and 50 are displayed for comparison. We find that $\mathcal{E}_k^i(k)\propto k^{-1.71}$ at $t=50$ over the inertial range $4\leqslant k\leqslant 25$, or equivalently, $0.25\leqslant\Lambda=2\pi/k\leqslant 1.57$, which closely follows Kolmogorov's spectrum, $\mathcal{E}_k^i(k)\propto k^{-5/3}$. This characterizes that, in the theory of CT, the inertial range is sustained by the Richardson cascade in which the energy is transferred from large to small scales without being dissipated. Our result implies that the Richardson cascade for quantized vortices occurs in the present system. Additionally, we note that lower and upper bounds of Λ correspond to the length scales characterizing the healing length and the size of the condensate, respectively, according to the previous investigations [9,14]. Our results are consistent with such a conclusion. However, the "size" of the condensate here should be addressed with care, since the pancake-shaped condensate possesses two characteristic sizes, namely, the radial and axial Thomas-Fermi radii, which are specified by $R_\perp=8$ and $R_z=R_\perp/\lambda=1.6$ in our model. Consequently, the numerical results reveal that the upper bound of Λ corresponds to R_z rather than $R_\perp$.

That $\mathcal{E}_k^i(k)$ consists with Kolmogorov's spectrum when time becomes large is of fundamental significance. This implies that a stable turbulent state can be achieved via the collapse of a single-vortex ring in a trapped BEC despite that no vorticity is injected into the system. It should be noted that this QT will decay eventually, but the relaxation time would be quite long due to the vortex-sound separation as shown below. To gain more insight into the essence of the QT in our model, we examine the spatial distribution of the incompressible and compressible kinetic energy densities, $\frac{1}{2}|(\sqrt{\rho}\nabla\varphi)^{i,c}|^2$, on the xy plane at $t=50$. In Fig. 4(a), the incompressible field is almost distributed over the rim of the atomic cloud. On the contrary, in Fig. 4(b) the compressible field spreads widely through the condensate. Apparently, the vortices characterized by the incompressible field tend to localize in the outer region of the condensate in the development of QT, which is a consequence of the mutual interaction between the vortex filaments emerging from the breakdown of the vortex ring. Unfortunately, the vortices localized in the outer region of the condensate are invisible in the isosurface, though hinted by wrinkled isosurface as shown in Fig. 2(l). To visualize the full spatial distribution of the vortices, we employ the so-called λ_2 method which en-

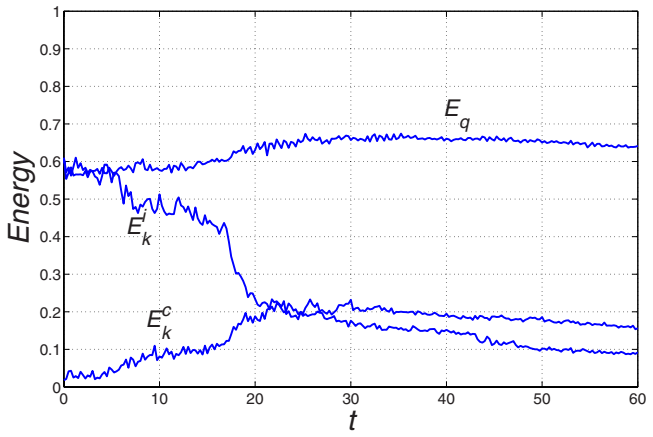

FIG. 5. (Color online) Time developments of E_q, E_k^i, and E_k^c.

ables one to identify the configuration of the vortices by locating the local pressure minima due to vortical motion [18]. In Figs. 4(c) and 4(d), the three-dimensional distribution of the vortices for $t=20$ and 50 are shown, respectively. Comparing with Fig. 2(k), where only a few vortices are present, we see that there are more vortices emerging in the outer region of the condensate as shown in Fig. 4(c). This means that those "disappeared" vortices in Fig. 2(k) are actually expelled to the periphery of the pancake-shaped atomic cloud where the density is much smaller compared with that of the central region. As time goes on, more vortex filaments of smaller sizes are gathered in the outer edge of condensate that can be visualized by comparing Fig. 4(c) and Fig. 4(d). In the meantime, these vortex filaments stir the condensate, cause the volume fluctuating, and wrinkle the density isosurface.

The time evolutions of different components of kinetic energies are shown for $0 \leqslant t \leqslant 60$ in Fig. 5. We see that E_k^c is overwhelmed by E_k^i initially, but as time goes on, E_k^i decreases as a portion of it continuously converts into E_k^c via vortex breakdown and vortex-sound interaction. Around $17 \leqslant t \leqslant 21$, the incompressible kinetic energy has an abrupt drop which is just about the period when broken vortex filaments are expelled to the periphery and the density isosurface begins to crinkle. Note that the total energy is conserved in our system. From the energy budget, the other part of the decrement of E_k^i mostly goes to E_{trap} and E_{int} as E_q changes little. This is especially so for $t>21$, because E_k^c is almost unchanged. The drop of E_k^i evidently corresponds to the continuous migration of broken vortex filaments to the outer low-density area of BEC. After that, the vortices and sound waves are spatially separated and the vortex-sound interaction is largely diminished as featured by the constancy of E_k^c after the drop. The energy of the vortex filaments at the circumference of the BEC continue to cascade, easily told by comparing Figs. 4(c) and 4(d), with its loss simply converting into the potential energy since cascade process obviously involves volume fluctuation of BEC. Consequently, we are able to obtain a state consistent with Kolmogorov spectrum without assuming any dissipative mechanism in our model. This is quite contrary to the conclusions of Refs. [9,14], in which a dissipation term must be introduced to suppress the short wave excitations in order to obtain the steady QT.

IV. CONCLUSIONS

In summary, we have investigated the quantum turbulence stemmed from the disruption of an unstable vortex ring in a pancaked-shaped BEC by the numerically solving the time-dependent GP equation. We verify that the incompressible kinetic energy spectrum of the turbulent state obeys Kolmogorov's $-5/3$ power law.

ACKNOWLEDGMENTS

This work is supported partially by National Center for Theoretical Sciences (NCTS), Hsinchu, Taiwan, and Taida Institute for Mathematical Sciences (TIMS), Taipei, Taiwan.

[1] R. J. Donnelly, *Quantized Vortices in Helium II* (Cambridge University Press, Cambridge, 1991).
[2] R. P. Feynman, *Progress in Low Temperature Physics*, edited by C. J. Gorter (North-Holland, Amsterdam, 1955).
[3] W. F. Vinen, Proc. R. Soc. London, Ser. A **240**, 114 (1957); **240**, 128 (1957); **240**, 493 (1957).
[4] J. Maurer and P. Tabeling, Europhys. Lett. **43**, 29 (1998).
[5] S. R. Stalp, L. Skrbek, and R. J. Donnelly, Phys. Rev. Lett. **82**, 4831 (1999).
[6] U. Frish, *Turbulence: The Legacy of A. N. Kolmogorov* (Cambridge University Press, Cambridge, 1995).
[7] T. Araki, M. Tsubota, and S. K. Nemirovskii, Phys. Rev. Lett. **89**, 145301 (2002).
[8] C. Nore, M. Abid, and M. E. Brachet, Phys. Rev. Lett. **78**, 3896 (1997); Phys. Fluids **9**, 2644 (1997).
[9] M. Kobayashi and M. Tsubota, Phys. Rev. Lett. **94**, 065302 (2005).
[10] L. Pitaevskii and S. Stringari, *Bose-Einstien Condensation* (Oxford University Press, Oxford, 2003).
[11] C. Lobo, A. Sinatra, and Y. Castin, Phys. Rev. Lett. **92**, 020403 (2004).
[12] N. G. Parker and C. S. Adams, Phys. Rev. Lett. **95**, 145301 (2005).
[13] A. A. Norrie, R. J. Ballagh, and C. W. Gardiner, Phys. Rev. Lett. **94**, 040401 (2005).
[14] M. Kobayashi and M. Tsubota, Phys. Rev. A **76**, 045603 (2007).
[15] T.-L. Horng, S.-C. Gou, and T.-C. Lin, Phys. Rev. A **74**, 041603(R) (2006).
[16] A. A. Svidzinsky and A. L. Fetter, Phys. Rev. A **62**, 063617 (2000).
[17] C.-H. Hsueh, S.-C. Gou, T.-L. Horng, and Y.-M. Kao, J. Phys. B **40**, 4561 (2007).
[18] J. Jeong and F. Hussain, J. Fluid Mech. **285**, 69 (1995).